Enhanced Thermoelectric Performance of As-Grown Suspended Graphene Nanoribbons

Qin-Yi Li,[*,†,⊥] Tianli Feng,[‡,§] Wakana Okita,[#] Yohei Komori,[†] Hiroo Suzuki,[#] Toshiaki Kato,[*,#,‖]
Toshiro Kaneko,[#] Tatsuya Ikuta,[†,⊥] Xiulin Ruan,[*,§] and Koji Takahashi[†,⊥]

[†]Department of Aeronautics and Astronautics, Kyushu University, Fukuoka 819-0395, Japan

[‡]Materials Science and Technology Division, Oak Ridge National Laboratory, Oak Ridge, Tennessee 37831, United States

[#]Department of Electronic Engineering, Tohoku University, Aoba 6-6-05, Aramaki, Aoba-ku, Sendai 980-8579, Japan

[§]School of Mechanical Engineering and the Birck Nanotechnology Center, Purdue University, West Lafayette, Indiana 47907-2088, United States

[‖]Japan Science and Technology Agency (JST)-PRESTO, Aoba 6-6-05, Aramaki, Aoba-ku, Sendai 980-8579, Japan

[⊥]International Institute for Carbon Neutral Energy Research (WPI-I2CNER), Kyushu University, Fukuoka 819-0395, Japan

Ⓢ *Supporting Information*

ABSTRACT: Conventionally, graphene is a poor thermoelectric material with a low figure of merit (ZT) of 10^{-4}–10^{-3}. Although nanostructuring was proposed to improve the thermoelectric performance of graphene, little experimental progress has been accomplished. Here, we carefully fabricated as-grown suspended graphene nanoribbons with quarter-micron length and ~40 nm width. The ratio of electrical to thermal conductivity was enhanced by 1−2 orders of magnitude, and the Seebeck coefficient was several times larger than bulk graphene, which yielded record-high ZT values up to ~0.1. Moreover, we observed a record-high electronic contribution of ~20% to the total thermal conductivity in the

nanoribbon. Concurrent phonon Boltzmann transport simulations reveal that the reduction of lattice thermal conductivity is mainly attributed to quasi-ballistic phonon transport. The record-high ratio of electrical to thermal conductivity was enabled by the disparate electron and phonon mean free paths as well as the clean samples, and the enhanced Seebeck coefficient was attributed to the band gap opening. Our work not only demonstrates that electron and phonon transport can be fundamentally tuned and decoupled in graphene but also indicates that graphene with appropriate nanostructures can be very promising thermoelectric materials.

KEYWORDS: suspended graphene nanoribbon, phonon transport, electrical conductivity, Seebeck coefficient, thermoelectricity
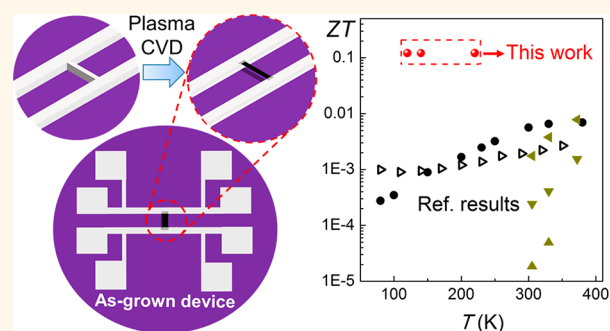
Thermoelectric materials can directly convert waste heat into electricity, and have attracted intense research efforts due to the huge demand of energy harvesting and power generation.[1−6] The efficiency of thermoelectric energy conversion is measured by the dimensionless figure of merit ZT that depends on the electrical conductivity σ, thermal conductivity k, Seebeck coefficient S, and the absolute temperature T, defined by $ZT = S^2\sigma T/k$. Thus, the enhancement of ZT can be achieved by increasing σ/k and S. However, since the parameters of ZT are generally coupled and difficult to manipulate, it has been very challenging to achieve $ZT > 1$ over the past half century.[1−3] Since the pioneering works of Hicks and Dresselhaus in 1993,[7,8] researchers have adopted the nanostructuring strategies to tune and decouple the parameters in ZT. An experimental breakthrough came out in 2008[1] where rough Si nanowires

held the same high electrical conductivity as the bulk, but 100-fold reduced thermal conductivity, leading to 1 order of magnitude enhancement of ZT (= 0.6). To date, nano-structured semiconductor compounds involving Bi, Te, Pb, Sb, and Ag deliver the highest ZT of 1.0−2.2,[1−3] but none of these compounds have been widely used in applications due to the high cost of these relatively rare or toxic elements.

Recently, researchers have witnessed rapidly growing interest in low-cost, nontoxic, light, and flexible thermoelectric materials[3−10] that are based on organic or nanocarbon materials, which is mainly driven by the emerging demand of powering small wireless devices like wearable electronics and
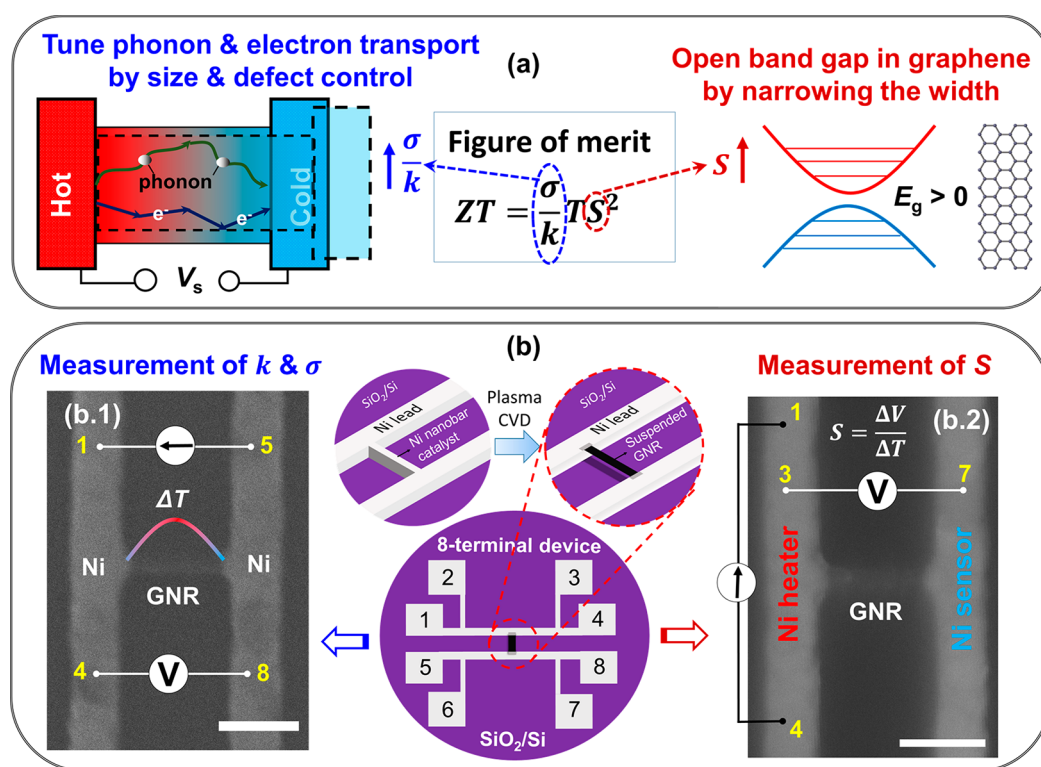
Figure 1. (a) Concept of how to enhance thermoelectric performance of graphene and (b) the as-grown test structure for the comprehensive thermoelectric measurements using an eight-terminal device. (b.1) thermal and electrical conductivity measurements illustrated in the SEM image; (b.2) thermopower measurement illustrated in the SEM image. Scale bars in (b.1) and (b.2) represent 200 nm.

remote sensors. For example, Avery and co-workers[5] doped semiconducting carbon nanotubes and enhanced their ZT from the order of 10^{-4}[11,12] to 0.01−0.05. As for graphene, despite its many attractive properties including lightness and softness, pristine graphene is a disappointingly poor thermoelectric material with ZT values as low as 10^{-4}−10^{-3},[13] because (1) its gapless band structure leads to a small Seebeck coefficient less than 100 μV/K[9] and (2) its superior electrical conductivity goes together with very high thermal conductivity, which leads to a very small σ/k ratio.[14−16] However, some theoretical studies[9,17−20] have demonstrated that appropriate nanostructuring of graphene can enhance the Seebeck coefficient *via* band gap opening and reduce the lattice thermal conductivity while preserving high electrical conductivity, which can yield $ZT > 1$ that is comparable to the best thermoelectric materials. However, little experimental progress has been made to effectively enhance ZT of graphene. Practical decoupling of electrical and thermal transport is extremely challenging, and suppression of thermal conductivity can easily lead to even greater reduction of electrical conductivity. Oh and co-workers[10] successfully fabricated nanostructured graphene meshes with largely reduced thermal conductivity and enhanced Seebeck coefficient, but the electrical conductivity was also significantly reduced. Eventually, the ZT of graphene nanomeshes[10] was even decreased by 1−2 orders of magnitude as compared to bulk graphene. In the present paper, we carefully fabricated as-grown free-standing graphene nanoribbons (GNRs) with quarter-micron lengths and low defects. We discovered record-high ratio of σ/k that is 1−2 orders of magnitude higher than those of previous graphene samples, and enhanced Seebeck coefficient as compared to bulk graphene. Thus, the ZT reached record-high values up to

~0.1, which can qualify properly nanostructured graphene as very promising thermoelectric materials.

RESULTS AND DISCUSSION

As-Grown Test Structure and Measurements. Suspended GNRs along with eight-terminal Ni films were synthesized by a recently developed rapid-heating plasma CVD method,[21,22] as shown in Figure 1b. The eight-terminal test structure allows measurements of the electrical and thermal conductivities (Figure 1b.1) and the Seebeck coefficient (Figure 1b.2) using the same device just by changing the outer circuit. In total, three GNR samples were fabricated on the same Si wafer in the same synthesis round. One of the samples was damaged during the wiring process, and the other two samples, *i.e.*, sample-1 and sample-2, were successfully measured for the electrical/thermal conductivities and the Seebeck coefficients, respectively. The details of the sample fabrication and measurement methods are provided in the Methods. Before the precise eight-terminal measurements, we conducted two-probe measurements of the source−drain current as a function of the back-gate voltage for all the three samples and proved that these high-quality samples on the same Si wafer should possess equivalent properties (Supplementary Note S9). There is no post process after GNR synthesis, so the as-grown suspended samples are free of polymer residue that is usually inevitable in other experiments involving graphene transfer, lithographical patterning, or post-electrode fabrication.[23,24] In addition, these plasma-CVD-grown GNRs should have low-disorder edges as previously demonstrated by polarized Raman spectroscopy,[21,22] while the other graphene nanostructures fabricated by top-down etching[10,25,26] had very rough edges that can strongly scatter
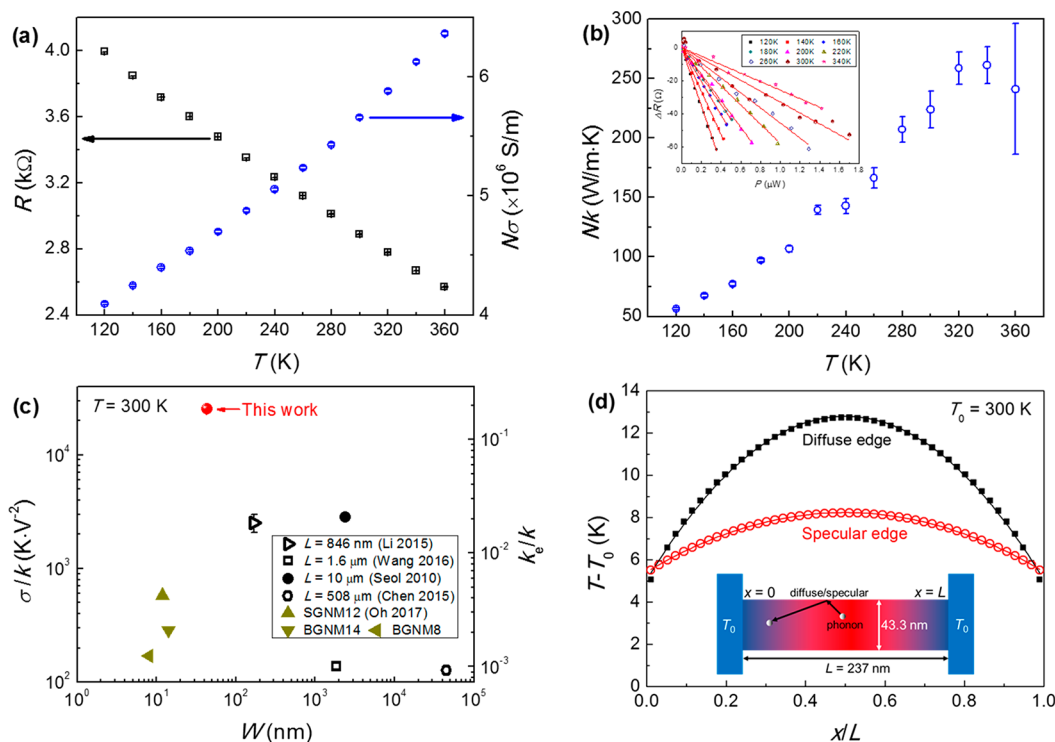
Figure 2. Record-high σ/k ratio of the GNR sample-1. (a) Electrical resistance and conductivity *versus* temperature; (b) thermal conductivity *versus* temperature (inset: change of resistance *versus* electrical power that was used to extract k); (c) the room-temperature σ/k ratio and k_e/k ratio compared with the reference data as a function of the (characteristic) width; (d) phonon Boltzmann transport simulation results that indicate quasi-ballistic phonon transport in the GNR, which explains the reduction of the thermal conductivity. In the figure legend of (c), SGNM and BGNM denote single-layer and bilayer graphene nanomeshes, respectively, and 12, 14, and 8 denote the neck width of the mesh in nm.

both phonons and electrons. Moreover, during the synthesis, the melted Ni thin film wrapped the GNR ends, which can ensure good electrical and thermal contacts.

Record-High Ratio of Electrical to Thermal Conductivity of GNR. The electrical and thermal conductivities of GNR sample-1 were measured in vacuum at 20 K steps between 120 and 360 K using a four-terminal electrical self-heating method (Figure 1b.1). This sample was 43.3 nm wide and 237.0 nm long, as measured in the SEM images (Supplementary Note S5). Although there is no simple way to determine the thickness of the suspended GNR, we have previously confirmed by cross-section TEM and Raman scattering spectra that the same plasma CVD process can produce both single- and few-layer GNRs.[21] We measured the electrical resistance as a function of temperature (Figure 2a) from the zero-power intercepts of the resistance-power ($R-P$) curves (Supplemental Note S1). The electrical resistance linearly deceases with increasing temperature, which indicates semiconductor behavior of this GNR. The electrical conductivity is defined by $\sigma = L/(RA) = L/(RWNt_1)$, where L and A are the sample length and cross sectional area, respectively, W the sample width, N the number of layers, and t_1 the thickness of single graphene layer (0.335 nm). Since we do not know the exact thickness of the sample (we will later demonstrate that sample-1 is probably single layer), we present the electrical conductivity multiplied by the layer number, *i.e.*, the $N\sigma$ product, in Figure 2a. Given that the thickness of the sample is less than five layers, its electrical conductivity is on the order of 10^6 S/m, among the highest values reported for graphene in the literature,[13,27−29] which confirms that the as-

grown sample is free of defects or impurities. The electrical current was elevated to provide Joule self-heating in the suspended GNR, and the average temperature rise of the GNR is determined by measuring the change of its electrical resistance. The electrical resistance displays a linear decreasing trend with increasing Joule power due to the negative dR/dT, and the linearity is better at lower temperatures (inset of Figure 2b and Supplementary Note S1).

According to Fourier's law, the temperature profile in the suspended GNR with uniform internal heat generation is parabolic with the two contacts kept at the heat sink temperature. The apparent thermal conductivity, k, is calculated from the measured average temperature rise under Joule heating, using the following formula:[30,34]

$$k = \frac{L}{12WNt_1}\frac{\Delta P}{\Delta T} = \frac{L}{12WNt_1}\frac{dR}{dT}\frac{dP}{dR} \quad (1)$$

The measured thermal conductivity multiplied by the layer number is plotted *versus* temperature in Figure 2b. The thermal conductivity increases with temperature until 320 K followed by a flattening trend, and this temperature dependence implies deviation from diffusive phonon transport[43−46] (Supplementary Note S4). Given that the sample is single layer (*i.e.*, $N = 1$), the thermal conductivity is (224 ± 16) W/mK at 300 K, only about 1/10 of that of large pristine graphene. Thus, the thermal conductivity is significantly reduced while the electrical conductivity is maintained at a high level. The ratio of electrical to thermal conductivity reached record-high values of $(2.27 \times 10^4)−(7.29 \times 10^4)$ K/V^2 at 120−360 K (Supplementary Note S3). Note that the assumption of the

thickness does not affect the value of σ/k since the layer number is canceled out in this ratio. As shown in Figure 2c, this σ/k ratio of the GNR is 1−2 orders of magnitude higher than those of both micrometer-sized graphene[13,31−33] with very high thermal conductivity of 2000 W/mK and graphene nanomeshes with very low thermal conductivity of ∼78 W/mK.[10]

Furthermore, the electrical conductivity can be converted to the electronic thermal conductivity, k_e, using the Wiedemann−Franz law, i.e., $k_e = \sigma T L_0$, where $L_0 = 2.44 \times 10^{-8}$ WΩ/K² is the standard Lorenz number that has been demonstrated to be applicable to graphene.[35] Then the lattice thermal conductivity, k_{ph}, is calculated by $k_{ph} = k - k_e$ (Supplementary Note S3), which equals (182 ± 16) W/mK at 300 K given that the sample is single layer. Conventionally, research in thermal transport in graphene has focused on the phononic (lattice) part, while the electronic contribution to thermal transport has been generally regarded as negligible. However, while the k_e/k ratio of previous graphene samples was measured to be less than 2% (Figure 2c), we observed that the as-grown ∼40 nm-wide GNR exhibited record-high electronic contribution of ∼20% to the total thermal conductivity at 120−360 K (Figure 2c and Supplementary Note S3), enhanced by a factor of 10−200 due to the large reduction of lattice thermal conductivity.

The reduction of the lattice thermal conductivity of this GNR as compared to bulk graphene may come from two possible effects: (1) narrow width induced reduction of phonon mean free path (mfp) due to boundary (edge) scattering and (2) short length induced quasi-ballistic effect. In the following, we will discuss which one dominates. The fraction of elastically scattered phonons at the edges can be characterized by the specularity parameter p that is determined by the edge roughness.[16,41] This specularity parameter is in the range of 0 (totally diffuse rough edge) to 1 (totally specular smooth edge). The phonon-boundary scattering induced mfp, λ_{ph-b}, is related to the specularity parameter by $\lambda_{ph-b} = W(1 + p)/(1 - p)$,[16,41] where W is the ribbon width and the phonon mfp in the GNR, λ_{ph}, can be approximated by the Matthiessen's rule[16] using $\lambda_{ph}^{-1} \approx \lambda_{bulk}^{-1} + \lambda_{ph-b}^{-1}$, where λ_{bulk} is the intrinsic phonon mfp in large pristine graphene.

The ballistic effect will result in temperature jumps at the ideal contacts due to the mixing of the ballistic cold phonons from heat sink and the ballistic hot phonons from heat source, which has been commonly observed in many physically detailed modeling no matter whether there is internal heat generation or not.[38−40] As part of the quasi-ballistic thermal transport that depends on the sample size, this temperature jump is an intrinsic phenomenon at nanoscale and is different from Kapitza resistance. It should not be removed from the measurements using either the self-heating approach or temperature-difference approach with no internal heat generation, like the k measurement of supported GNRs by Bae et al.;[26] otherwise, the measured thermal conductivity will be the bulk value. At nanoscale, different measurement methods including the contact and noncontact ones[35−40] can yield essentially different apparent thermal conductivity based on the Fourier's law. In practical applications, we can use the Fourier's law by adopting a size-dependent apparent thermal conductivity, but we need to identify the appropriate k measurement method for specific applications. Graphene is driven with current in most applications including thermoelectrics; thus our electrical self-heating measurement of k is

indispensable and the extracted apparent thermal conductivity can be well-defined using the Fourier's law.

To capture the details of phonon transport in the suspended GNR, we did finite volume method (FVM) simulations for the phonon Boltzmann transport equation (BTE) for the 43.3 nm wide, 237 nm long sample with uniform internal heat generation.[38,42] We obtained the temperature profile along the GNR, i.e., $T(x)$, from which the apparent thermal conductivity, k_{app}, is calculated using the following definition[38,40]

$$k_{app} = \frac{qL^2}{12(\langle T(x) - T_0 \rangle)} \qquad (2)$$

where q is the volumetric heat generation rate, L is the sample length, T_0 is the heat sink temperature, and $\langle T(x) - T_0 \rangle$ is the volumetric average temperature rise. The details of the BTE simulations along with the input parameters are elaborated in the Methods and Supplementary Note S7.

We considered two extreme cases for the edge scattering, i.e., the diffuse edges where all phonons are diffusely scattered, and the specular edges where all phonons are elastically scattered. With the internal heat power $P = 1$ μW at 300 K, the temperature profiles are plotted along the normalized length in Figure 2d. The temperature profiles for both cases are parabolic curves that peak at the middle of the sample, which agrees with the Fourier's law prediction. The temperature jumps at the contacts are originated from quasi-ballistic phonon transport. The temperature jump is 5.05 K for the diffuse edge and 5.44 K for the specular edge, and the average temperature rise is 10.22 K for the diffuse edge and 7.30 K for the specular case. Using eq 2, we calculate the apparent thermal conductivity to be 133 W/mK for the diffuse edge and 186 W/mK for the specular case. This BTE-calculated k for the specular case is very close to our measured lattice thermal conductivity $[(182 \pm 16)$ W/mK at 300 K] given our sample is single-layer, which indicates very weak phonon-edge scattering in our as-grown GNR.

Next, we examine the possibility of multilayer thickness. If the sample is multilayer, the measured lattice thermal conductivity should be 60.7 ± 5.3 W/mK for the trilayer case and 36.4 ± 3.2 W/mK for the five-layer case at 300 K. To have these low thermal conductivities, BTE simulations show that the corresponding bulk value of phonon mfp should be 14.4 nm for the trilayer case and 5.4 nm for the five-layer case even for totally diffuse edges (Supplementary Note S7). These bulk phonon mfps are 1 to 2 orders of magnitude lower than that of pristine graphene (282 nm, see Supplementary Note S7), indicating high density of bulk defects if we assume the sample is multilayer. This is contradictory to the high sample quality that is guaranteed by the as-grown process and proved by the high electrical conductivity which is on the order of 10^6 S/m. Therefore, our measured sample is very possibly single layer according to the phonon BTE calculations, and the quasi-ballistic phonon transport instead of phonon-edge scattering is the main reason for the reduction of lattice thermal conductivity.

Now we discuss on why the ratio of electrical to thermal conductivity of our quarter-micron long GNR is orders of magnitude higher than those of previous samples, which significantly contributes to the record-high thermoelectric performance. Since many factors can suppress both σ and k, the enhancement of the σ/k ratio can only be achieved by
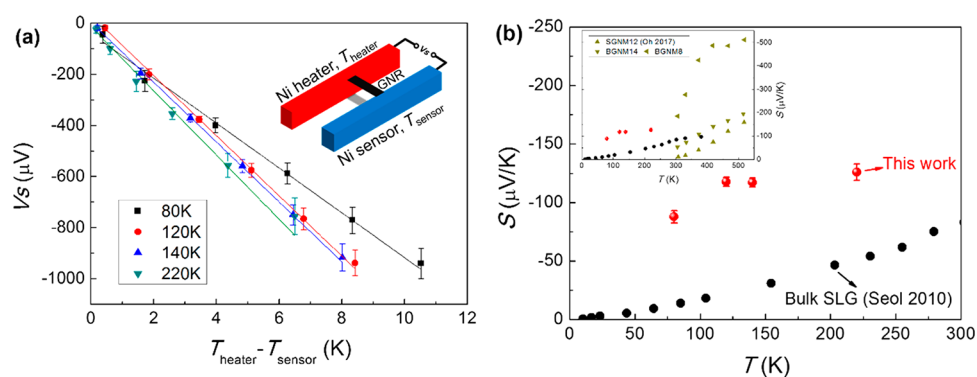
Figure 3. Thermopower measurements of GNR sample-2. (a) Seebeck voltages as a function of the temperature difference between the Ni heater and sensor (inset: schematic illustration of the measurement method). (b) Seebeck coefficients of this GNR and bulk single-layer graphene (SLG)[13] below 300 K, plotted in the reversed coordinate. The inset in (b) includes the Seebeck coefficients of graphene nanomeshes above 300 K.[10]

properly decoupling the influencing factors on both phonon and electron transports. The first reason for the record-high σ/k ratio of our GNR is the low level of bulk defects or impurities that is enabled by the as-grown synthesis, which leads to a very high electrical conductivity. Theoretical studies have predicted that bulk defects and impurities will suppress electron transport more significantly than phonon transport,[18,19] while these defects and impurities are inevitable and relatively high in the reference samples that are not as grown, which explains the reduced σ/k ratio of the reference samples. Given our sample is monolayer, its electrical conductivity is up to 5.66×10^6 S/m at 300 K and among the highest values reported for graphene and GNRs,[27−29] and the electron mobility would be 6×10^4 cm^2 V^{-1} s^{-1} if we assume a carrier concentration of 2×10^{11} cm^{-2}.[13,27] The high electron mobility is mainly attributed to the weak electron scattering with defects, impurities or edge disorder of the high-quality as-grown samples and also enabled by the suspension geometry that eliminated the substrate suppression on electron transport.[13,27] The second reason for the record-high σ/k is the disparate phonon and electron mean free paths (mfps) that lead to different effects of the short length on electron and phonon transport. The quarter-micron length of our sample strongly reduced the lattice thermal conductivity due to the quasi-ballistic phonon transport, while the electrical conductivity was much less affected by the sample length because the phonon mfp (282 nm) is much longer than the electron mfp (~50 nm).[26,47] The relatively smooth edges may have also contributed to the enhancement of σ/k, since the low level of edge disorder can still scatter phonons but have a negligible effect on electrons in GNRs, as predicted by the theoretical work of Haskins and co-workers.[19] In addition, both electron and phonon transport can be suppressed by the substrate,[13,27,48] but for GNRs, it is still unclear whether the substrate effect is more pronounced on phonons than electrons or otherwise. Thus, whether the free-standing structure in this work is favorable or not for the enhancement of σ/k remains an open question for future research.

Enhanced Seebeck Coefficient and Record-High Figure of Merit. The Seebeck coefficients of GNR sample-2 (Figure 1b.2, 37.8 nm wide and 278.0 nm long) were measured using an eight-terminal method (see Methods and Supplementary Note S8). The GNR bridges a Ni heater and sensor, and Figure 3a plots the measured Seebeck voltages, V_s, as a function of the temperature difference between the two ends of the GNR, i.e., $T_{heater} - T_{sensor}$. The error bars indicate the

random uncertainties based on six measurements. The Seebeck coefficient S was obtained by linear fitting of the $V_s - (T_{heater} - T_{sensor})$ data, i.e., $S = dV_s/d(T_{heater} - T_{sensor})$. Figure 3b compares our measured Seebeck coefficients of the GNR at 80−220 K with those of supported bulk graphene[13] and graphene nanomeshes.[10] The Seebeck coefficient of our GNR changes from $(-87.7 \pm 5.2)-(-125.7 \pm 7.1)$ μV/K as the temperature increases from 80 to 220 K, which are enhanced by a factor of 2−6 as compared to bulk graphene at the corresponding temperatures. The enhanced thermopower in nanostructured graphene is mainly attributed to the opening of the band gap.[9,10] Compared with the reported graphene nanomeshes, only the bilayer graphene nanomesh with a neck width of 8 nm (BGNM8) tends to exhibit a much larger thermopower than our sample, but its σ/k ratio is 2 orders of magnitude lower than that of our GNR (Figure 2c); thus, the overall ZT value of the reported graphene nanostructures should be much lower than that of our as-grown samples.

We combined the measured electrical and thermal conductivities of sample-1 and the Seebeck coefficients of sample-2 to estimate the figure of merit of the as-grown 40 nm wide GNRs to be about 0.12 at 120−220 K. The room-temperature (rt) ZT of our GNR samples should also be no less than 0.1 if we reasonably assume the rt Seebeck coefficient to be no less than -120 μV/K. As shown in Figure 4, this ZT value is 2−4 orders of magnitude higher than all the reported ZT values of graphene-based materials including bulk graphene,[13] nanomeshed,[10] and doped graphene.[49] In addition, the ZT value of the as-grown GNRs is also orders of magnitude
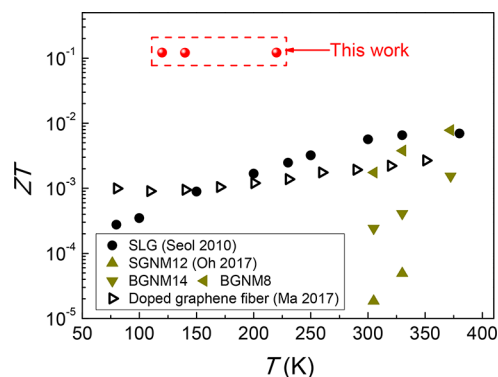
Figure 4. Record-high ZT of the suspended GNR.

higher than the reported values of undoped single- and multiwalled CNTs, which range from 10^{-7} to 10^{-4}.[11,12] Until now, the highest ZT value for nanocarbon-based materials has been reported to be 0.157 in n-type-doped CNTs,[3,50] while most other doped CNTs exhibited a ZT value around 0.01.[3,5] Therefore, the ZT value of the as-grown quarter-micron long GNRs is not only record high for graphene based materials, but also among the highest of all the nanocarbon-based materials.

CONCLUSIONS

In summary, we have carefully fabricated as-grown suspended GNRs with 40 nm width and quarter-micron length and comprehensively measured the electrical conductivity, thermal conductivity, and Seebeck coefficient. We observed record-high ratio of electrical to thermal conductivity or equivalently record-high electronic contribution of ~20% to the total thermal conductivity, which is 1−2 orders of magnitude higher than the reported values of graphene and related nanostructures. Phonon Boltzmann transport simulations reveal that the enhancement of σ/k is mainly attributed to disparate electron and phonon mean free paths as well as the defect-free samples. The Seebeck coefficient of the GNR was also several times larger than that of bulk graphene. As a result, the as-grown GNRs exhibited a record-high ZT value of ~0.1, which is 2−4 orders of magnitude higher than that of other graphene based materials. Our work demonstrates that the electron and phonon transports can be fundamentally tuned and decoupled by size and defect control and highlights defect-free graphene with appropriate nanostructures as very promising thermoelectric materials.

METHODS

Sample Fabrication. Some details of the plasma CVD process were explained as follows. First, using the electron-beam lithography followed by Ni deposition, we fabricated a ~50 nm wide, ~70 nm thick Ni nanobar catalyst along with Ni heater, sensor, and electrodes on a SiO_2/Si wafer. Then the substrate was put in the electric furnace for the rapid-heating plasma CVD, during which the Ni nanobar catalyst melted and dewetted to the electrodes, leaving the above GNR free-standing, ready for thermal conductivity and thermopower measurements. More details of the plasma CVD synthesis can be found in refs.[21,22]

Thermal Conductivity and Thermopower Measurements. The samples were loaded into a liquid-nitrogen cooled cryostat for thermal and thermopower measurements under high vacuum ($<3 \times 10^{-4}$ Pa). The electrical resistance of the GNR was measured at varying electrical power using the four-terminal scheme (Figure 1b), and the thermal conductivity was extracted from the Joule-heating induced temperature rise that is determined from the resistance–temperature relationship. The instrumentation and details are elaborated in Supplementary Note S1.

The Seebeck coefficient was measured using an eight-terminal method. As illustrated in Figure 1b and the inset of Figure 3a, the GNR bridges two long Ni films, one of which acts as the heater while the other acts as the sensor. The Ni heater was driven with high DC current to establish a temperature difference across the GNR, and the temperatures of both the heater and sensor were measured from their resistance using the four-terminal scheme. At the same time, the Seebeck voltage was measured across the GNR after canceling out the voltage drop in the Ni heater. More details of the thermopower measurements are provided in Supplementary Note S8.

Phonon BTE Simulations. The phonon BTE was solved for the 43.3 nm wide and 237 nm long suspended GNR using the finite volume method. The input parameters in the BTE simulation code include the sample sizes, internal heat generation rate, specific heat, phonon group velocity, and bulk mean free path (mfp). The specific

heat was calculated from the phonon density of states. The phonon group velocity was calculated from the phonon dispersion relation of graphene. The intrinsic bulk phonon mfp was calculated to be $\lambda_{bulk} = 282$ nm from the bulk thermal conductivity of graphene, which is taken as $k_{bulk} = 2000$ W/mK.[51] More details of the phonon BTE simulations are provided in Supplementary Note S7.

ASSOCIATED CONTENT

Ⓢ Supporting Information

The Supporting Information is available free of charge on the ACS Publications website at DOI: 10.1021/acsnano.9b03521.

Details of the thermal conductivity measurement; comparison of the measured electrical and thermal conductivities with the references; record-high electronic contribution to thermal transport; discussion on the temperature dependence of the measured thermal conductivity; SEM images of GNR sample-1 after burnout; uncertainty analysis for the thermal conductivity measurements; details of the phonon BTE simulations; details of the Seebeck coefficient measurement; back-gate measurements for the three samples on the same wafer (PDF)

AUTHOR INFORMATION

Corresponding Authors
*E-mail: qinyi.li@aero.kyushu-u.ac.jp.
*E-mail: kato12@ecei.tohoku.ac.jp.
*E-mail: ruan@purdue.edu.

ORCID Ⓞ
Qin-Yi Li: 0000-0003-1388-7686
Tianli Feng: 0000-0002-7284-5657
Xiulin Ruan: 0000-0001-7611-7449
Koji Takahashi: 0000-0002-3552-9292

Notes
The authors declare no competing financial interest.

REFERENCES

(1) Hochbaum, A. I.; Chen, R.; Delgado, R. D.; Liang, W.; Garnett, E. C.; Najarian, M.; Majumdar, A.; Yang, P. Enhanced Thermoelectric Performance of Rough Silicon Nanowires. *Nature* **2008**, *451*, 163.

(2) Heremans, J. P.; Dresselhaus, M. S.; Bell, L. E.; Morelli, D. T. When Thermoelectrics Reached the Nanoscale. *Nat. Nanotechnol.* **2013**, *8*, 471.

(3) Blackburn, J. L.; Ferguson, A. J.; Cho, C.; Grunlan, J. C. Carbon-Nanotube-Based Thermoelectric Materials and Devices. *Adv. Mater.* **2018**, *30*, 1704386.

(4) Bahk, J. H.; Fang, H.; Yazawa, K.; Shakouri, A. Flexible Thermoelectric Materials and Device Optimization for Wearable Energy Harvesting. *J. Mater. Chem. C* **2015**, *3*, 10362−10374.

(5) Avery, A. D.; Zhou, B. H.; Lee, J.; Lee, E. S.; Miller, E. M.; Ihly, R.; Wesenberg, D.; Mistry, K. S.; Guillot, S. L.; Zink, B. L.; Kim, Y.-

H.; Blackburn, J. L.; Ferguson, A. J. Tailored Semiconducting Carbon Nanotube Networks with Enhanced Thermoelectric Properties. *Nat. Energy* **2016**, *1*, 16033.

(6) Jin, Q.; Jiang, S.; Zhao, Y.; Wang, D.; Qiu, J.; Tang, D. M.; Tan, J.; Sun, D.-M.; Hou, P.-X.; Chen, X.-Q.; Tai, K.; Gao, N.; Liu, C.; Cheng, H.-M.; Jiang, X. Flexible Layer-Structured Bi₂Te₃ Thermoelectric on a Carbon Nanotube Scaffold. *Nat. Mater.* **2019**, *18*, 62.

(7) Hicks, L. D.; Dresselhaus, M. S. Effect of Quantum-Well Structures on the Thermoelectric Figure of Merit. *Phys. Rev. B: Condens. Matter Mater. Phys.* **1993**, *47*, 12727.

(8) Hicks, L. D.; Dresselhaus, M. S. Thermoelectric Figure of Merit of a One-Dimensional Conductor. *Phys. Rev. B: Condens. Matter Mater. Phys.* **1993**, *47*, 16631.

(9) Dollfus, P.; Nguyen, V. H.; Saint-Martin, J. Thermoelectric Effects in Graphene Nanostructures. *J. Phys.: Condens. Matter* **2015**, *27*, 133204.

(10) Oh, J.; Yoo, H.; Choi, J.; Kim, J. Y.; Lee, D. S.; Kim, M. J.; Lee, J.-C.; Kim, W.-N.; Grossman, J. C.; Park, J. H.; Lee, S. S.; Kim, H.; Son, J. G. Significantly Reduced Thermal Conductivity and Enhanced Thermoelectric Properties of Single- and Bi-Layer Graphene Nanomeshes with Sub-10 nm Neck-Width. *Nano Energy* **2017**, *35*, 26−35.

(11) Shi, L.; Li, D.; Yu, C.; Jang, W.; Kim, D.; Yao, Z.; Kim, P.; Majumdar, A. Measuring Thermal and Thermoelectric Properties of One-Dimensional Nanostructures Using a Microfabricated Device. *J. Heat Transfer* **2003**, *125*, 881−888.

(12) Miao, T.; Shi, S.; Yan, S.; Ma, W.; Zhang, X.; Takahashi, K.; Ikuta, T. Integrative Characterization of the Thermoelectric Performance of an Individual Multiwalled Carbon Nanotube. *J. Appl. Phys.* **2016**, *120*, 124302.

(13) Seol, J. H.; Jo, I.; Moore, A. L.; Lindsay, L.; Aitken, Z. H.; Pettes, M. T.; Li, X.; Yao, Z.; Huang, R.; Broido; Mingo, N. Two-Dimensional Phonon Transport in Supported Graphene. *Science* **2010**, *328*, 213−216.

(14) Balandin, A. A. Thermal Properties of Graphene and Nanostructured Carbon Materials. *Nat. Mater.* **2011**, *10*, 569.

(15) Pop, E.; Varshney, V.; Roy, A. K. Thermal Properties of Graphene: Fundamentals and Applications. *MRS Bull.* **2012**, *37*, 1273−1281.

(16) Gu, X.; Wei, Y.; Yin, X.; Li, B.; Yang, R. Phononic Thermal Properties of Two-Dimensional Materials. *arXiv:1705.06156* https://arxiv.org/abs/1705.06156 (accessed May 16, 2017).

(17) Sevinçli, H.; Cuniberti, G. Enhanced Thermoelectric Figure of Merit in Edge-Disordered Zigzag Graphene Nanoribbons. *Phys. Rev. B: Condens. Matter Mater. Phys.* **2010**, *81*, 113401.

(18) Ouyang, Y.; Guo, J. A Theoretical Study on Thermoelectric Properties of Graphene Nanoribbons. *Appl. Phys. Lett.* **2009**, *94*, 263107.

(19) Haskins, J.; Kınacı, A.; Sevik, C.; Sevinçli, H.; Cuniberti, G.; Çağın, T. Control of Thermal and Electronic Transport in Defect-Engineered Graphene Nanoribbons. *ACS Nano* **2011**, *5*, 3779−3787.

(20) Yamawaki, M.; Ohnishi, M.; Ju, S.; Shiomi, J. Multifunctional Structural Design of Graphene Thermoelectrics by Bayesian Optimization. *Sci. Adv.* **2018**, *4*, No. eaar4192.

(21) Kato, T.; Hatakeyama, R. Site- and Alignment-Controlled Growth of Graphene Nanoribbons from Nickel Nanobars. *Nat. Nanotechnol.* **2012**, *7*, 651.

(22) Suzuki, H.; Kaneko, T.; Shibuta, Y.; Ohno, M.; Maekawa, Y.; Kato, T. Wafer-Scale Fabrication and Growth Dynamics of Suspended Graphene Nanoribbon Arrays. *Nat. Commun.* **2016**, *7*, 11797.

(23) Pettes, M. T.; Jo, I.; Yao, Z.; Shi, L. Influence of Polymeric Residue on the Thermal Conductivity of Suspended Bilayer Graphene. *Nano Lett.* **2011**, *11*, 1195−1200.

(24) Jo, I.; Pettes, M. T.; Lindsay, L.; Ou, E.; Weathers, A.; Moore, A. L.; Yao, Z.; Shi, L. Reexamination of Basal Plane Thermal Conductivity of Suspended Graphene Samples Measured by Electro-Thermal Micro-Bridge Methods. *AIP Adv.* **2015**, *5*, 053206.

(25) Liao, A. D.; Wu, J. Z.; Wang, X.; Tahy, K.; Jena, D.; Dai, H.; Pop, E. Thermally Limited Current Carrying Ability of Graphene Nanoribbons. *Phys. Rev. Lett.* **2011**, *106*, 256801.

(26) Bae, M. H.; Li, Z.; Aksamija, Z.; Martin, P. N.; Xiong, F.; Ong, Z. Y.; Knezevic, I.; Pop, E. Ballistic to Diffusive Crossover of Heat Flow in Graphene Ribbons. *Nat. Commun.* **2013**, *4*, 1734.

(27) Bolotin, K. I.; Sikes, K. J.; Jiang, Z.; Klima, M.; Fudenberg, G.; Hone, J.; Kim, P.; Stormer, H. L. Ultrahigh Electron Mobility in Suspended Graphene. *Solid State Commun.* **2008**, *146*, 351−355.

(28) Bolotin, K. I. Electronic Transport in Graphene: Towards High Mobility. In *Graphene*; Woodhead Publishing, 2014; pp 199−227.

(29) Han, M. Y.; Özyilmaz, B.; Zhang, Y.; Kim, P. Energy Band-Gap Engineering of Graphene Nanoribbons. *Phys. Rev. Lett.* **2007**, *98*, 206805.

(30) Li, Q. Y.; Takahashi, K.; Ago, H.; Zhang, X.; Ikuta, T.; Nishiyama, T.; Kawahara, K. Temperature Dependent Thermal Conductivity of A Suspended Submicron Graphene Ribbon. *J. Appl. Phys.* **2015**, *117*, 065102.

(31) Chen, L.; Xie, H.; Yu, W.; Wang, B.; Wu, Z. Thermal Transport Behaviors of Suspended Graphene Sheets with Different Sizes. *Int. J. Therm. Sci.* **2015**, *94*, 221−227.

(32) Wang, H.; Kurata, K.; Fukunaga, T.; Ago, H.; Takamatsu, H.; Zhang, X.; Ikuta, T.; Takahashi, K.; Nishiyama, T.; Takata, Y. Simultaneous Measurement of Electrical and Thermal Conductivities of Suspended Monolayer Graphene. *J. Appl. Phys.* **2016**, *119*, 244306.

(33) Wang, H.; Kurata, K.; Fukunaga, T.; Zhang, X.; Takamatsu, H. Width Dependent Intrinsic Thermal Conductivity of Suspended Monolayer Graphene. *Int. J. Heat Mass Transfer* **2017**, *105*, 76−80.

(34) Raja, S. N.; Rhyner, R.; Vuttivorakulchai, K.; Luisier, M.; Poulikakos, D. Length Scale of Diffusive Phonon Transport in Suspended Thin Silicon Nanowires. *Nano Lett.* **2017**, *17*, 276−283.

(35) Vallabhaneni, A. K.; Singh, D.; Bao, H.; Murthy, J.; Ruan, X. Reliability of Raman Measurements of Thermal Conductivity of Single-Layer Graphene due to Selective Electron-Phonon Coupling: A First-Principles Study. *Phys. Rev. B: Condens. Matter Mater. Phys.* **2016**, *93*, 125432.

(36) Li, Q. Y.; Xia, K.; Zhang, J.; Zhang, Y.; Li, Q.; Takahashi, K.; Zhang, X. Measurement of Specific Heat and Thermal Conductivity of Supported and Suspended Graphene by A Comprehensive Raman Optothermal Method. *Nanoscale* **2017**, *9*, 10784−10793.

(37) Sullivan, S.; Vallabhaneni, A.; Kholmanov, I.; Ruan, X.; Murthy, J.; Shi, L. Optical Generation and Detection of Local Nonequilibrium Phonons in Suspended Graphene. *Nano Lett.* **2017**, *17*, 2049−2056.

(38) Kaiser, J.; Feng, T.; Maassen, J.; Wang, X.; Ruan, X.; Lundstrom, M. Thermal Transport at the Nanoscale: A Fourier's Law *vs.* Phonon Boltzmann Equation Study. *J. Appl. Phys.* **2017**, *121*, 044302.

(39) Maassen, J.; Lundstrom, M. Steady-State Heat Transport: Ballistic-to-Diffusive with Fourier's Law. *J. Appl. Phys.* **2015**, *117*, 035104.

(40) Hua, Y. C.; Cao, B. Y. The Effective Thermal Conductivity of Ballistic−Diffusive Heat Conduction in Nanostructures with Internal Heat Source. *Int. J. Heat Mass Transfer* **2016**, *92*, 995−1003.

(41) Nika, D. L.; Askerov, A. S.; Balandin, A. A. Anomalous Size Dependence of the Thermal Conductivity of Graphene Ribbons. *Nano Lett.* **2012**, *12*, 3238−3244.

(42) Bao, H.; Chen, J.; Gu, X.; Cao, B. A Review of Simulation Methods in Micro/Nanoscale Heat Conduction. *ES Energy Environ* **2018**, *1*, 16−55.

(43) Feng, T.; Ruan, X. Four-Phonon Scattering Reduces Intrinsic Thermal Conductivity of Graphene and the Contributions from Flexural Phonons. *Phys. Rev. B: Condens. Matter Mater. Phys.* **2018**, *97*, 045202.

(44) Xu, X.; Wang, Y.; Zhang, K.; Zhao, X.; Bae, S.; Heinrich, M.; Bui, C. T.; Xie, R.; Thong, J. T. L.; Hong, B. H.; Loh, K. P.; Li, B.; Oezyilmaz, B. Phonon Transport in Suspended Single Layer Graphene. *arXiv:1012.2937*, https://arxiv.org/abs/1012.2937 (accessed Dec 14, 2010).

(45) Munoz, E.; Lu, J.; Yakobson, B. I. Ballistic Thermal Conductance of Graphene Ribbons. *Nano Lett.* **2010**, *10*, 1652−1656.

(46) Wang, Z.; Xie, R.; Bui, C. T.; Liu, D.; Ni, X.; Li, B.; Thong, J. T. Thermal Transport in Suspended and Supported Few-Layer Graphene. *Nano Lett.* **2011**, *11*, 113−118.

(47) Kim, T. Y.; Park, C. H.; Marzari, N. The Electronic Thermal Conductivity of Graphene. *Nano Lett.* **2016**, *16*, 2439−2443.

(48) Chen, J.; Zhang, G.; Li, B. Substrate Coupling Suppresses Size Dependence of Thermal Conductivity in Supported Graphene. *Nanoscale* **2013**, *5*, 532−536.

(49) Ma, W.; Liu, Y.; Yan, S.; Miao, T.; Shi, S.; Xu, Z.; Zhang, X.; Gao, C. Chemically Doped Macroscopic Graphene Fibers with Significantly Enhanced Thermoelectric Properties. *Nano Res.* **2018**, *11*, 741−750.

(50) Fukumaru, T.; Fujigaya, T.; Nakashima, N. Development of n-Type Cobaltocene-Encapsulated Carbon Nanotubes with Remarkable Thermoelectric Property. *Sci. Rep.* **2015**, *5*, 7951.

(51) Xu, X.; Pereira, L. F.; Wang, Y.; Wu, J.; Zhang, K.; Zhao, X.; Bae, S.; Bui, C. T.; Xie, R.; Thong, J. T. L.; Hong, B. H.; Loh, K. P.; Donadio, D.; Li, B.; Özyilmaz, B. Length-Dependent Thermal Conductivity in Suspended Single-Layer Graphene. *Nat. Commun.* **2014**, *5*, 3689.